

Anomalous compression behavior of germanium during phase transformation

Xiaozhi Yan, Dayong Tan, Xiangting Ren, Wenge Yang, Duanwei He, and Ho-Kwang Mao

Citation: [Applied Physics Letters](#) **106**, 171902 (2015); doi: 10.1063/1.4919003

View online: <http://dx.doi.org/10.1063/1.4919003>

View Table of Contents: <http://scitation.aip.org/content/aip/journal/apl/106/17?ver=pdfcov>

Published by the [AIP Publishing](#)

Articles you may be interested in

[Mechanical behaviors and phase transition of Ho₂O₃ nanocrystals under high pressure](#)

J. Appl. Phys. **116**, 033507 (2014); 10.1063/1.4890341

[New high-pressure phase and equation of state of Ce₂Zr₂O₈](#)

J. Appl. Phys. **111**, 053519 (2012); 10.1063/1.3692807

[High-pressure phase transitions and compressibility of wolframite-type tungstates](#)

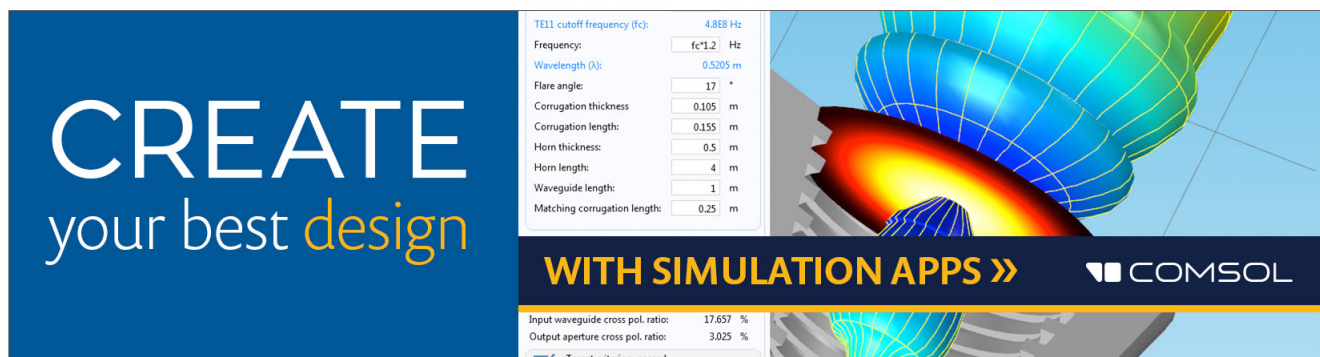
J. Appl. Phys. **107**, 083506 (2010); 10.1063/1.3380848

[Rate-dependent phase transformations in nanoindented germanium](#)

J. Appl. Phys. **105**, 126101 (2009); 10.1063/1.3151967

[The high-pressure phase behavior and compressibility of 2,4,6-trinitrotoluene](#)

Appl. Phys. Lett. **93**, 081912 (2008); 10.1063/1.2973162

An advertisement for COMSOL simulation software. On the left, a blue box contains the text 'CREATE your best design' in white and yellow. On the right, a 3D simulation of a horn antenna is shown with a color-coded field distribution. A control panel on the left lists parameters: TE11 cutoff frequency (fc): 4.868 Hz; Frequency: fc*1.2 Hz; Wavelength (lambda): 0.5205 m; Flare angle: 17 degrees; Corrugation thickness: 0.105 m; Corrugation length: 0.155 m; Horn thickness: 0.5 m; Horn length: 4 m; Waveguide length: 1 m; Matching corrugation length: 0.25 m. At the bottom, it says 'WITH SIMULATION APPS >>' and the COMSOL logo. Below the parameters, it shows 'Input waveguide cross pol. ratio: 17.657 %', 'Output aperture cross pol. ratio: 3.025 %', and a checked box for 'Target criterion: passed'.

Anomalous compression behavior of germanium during phase transformation

Xiaozhi Yan,^{1,2} Dayong Tan,^{2,3} Xiangting Ren,² Wenge Yang,^{2,4,a)} Duanwei He,^{1,5,a)} and Ho-Kwang Mao^{2,4,6}

¹Institute of Atomic and Molecular Physics, Sichuan University, Chengdu 610065, People's Republic of China

²Center for High Pressure Science and Technology Advanced Research (HPSTAR), Shanghai 201203, People's Republic of China

³Guangzhou Institute of Geochemistry, Chinese Academic of Sciences, Guangzhou 510640, People's Republic of China

⁴High Pressure Synergetic Consortium (HPSynC), Geophysical Laboratory, Carnegie Institution of Washington, Argonne, Illinois 60439, USA

⁵Institute of Fluid Physics and National Key Laboratory of Shockwave and Detonation Physics, China Academy of Engineering Physics, Mianyang 621900, People's Republic of China

⁶Geophysical Laboratory, Carnegie Institution of Washington, Washington, DC 20015, USA

(Received 4 February 2015; accepted 14 April 2015; published online 27 April 2015)

In this article, we present the abnormal compression and plastic behavior of germanium during the pressure-induced cubic diamond to β -tin structure transition. Between 8.6 GPa and 13.8 GPa, in which pressure range both phases are co-existing, first softening and followed by hardening for both phases were observed via synchrotron x-ray diffraction and Raman spectroscopy. These unusual behaviors can be interpreted as the volume misfit between different phases. Following Eshelby, the strain energy density reaches the maximum in the middle of the transition zone, where the switch happens from softening to hardening. Insight into these mechanical properties during phase transformation is relevant for the understanding of plasticity and compressibility of crystal materials when different phases coexist during a phase transition. © 2015 AIP Publishing LLC.

[<http://dx.doi.org/10.1063/1.4919003>]

During a pressure-induced transformation from one solid phase to another, usually both phases can co-exist over a certain pressure range with increasing fraction of the new phase while the transition progresses. The crystal structure and lattice parameters of the new phase are different from the original phase, thus, strain energy is generated during nucleation and growth of new phase to accommodate the misfit between the nucleus and the matrix as the portion of new phase grows. This strain energy leads to the modification of the system's compression behaviors, for example, mechanical properties and phase transition process.¹⁻⁵ When the external pressure applies to the mixed phase system, the elasticity and plasticity of the nucleus and matrix could behave differently from both phases, due to the additional internal strain between them.

Traditional tensile test shows unusual deformation behavior of materials during phase transition, namely, "transformation plasticity."^{6,7} By modeling the plastic behavior of each phase associated with the internal stress caused by the volumetric strain during phase transition, various theories have been proposed to interpret the observations.^{1,7} However, the plasticity observed in the reported experiments comes from the mixture of two phases, instead of a pure single phase. The proposed models have not been well examined directly by *in situ* experiments. Besides, the plastic behavior of material during the pressure-induced phase transition has been largely ignored. Here, we present the *in-situ* high-pressure studies on the plasticity and compressibility of germanium using

synchrotron X-ray diffraction (XRD) technique. During the phase transition from diamond structure (Ge-I) to metallic β -tin phase (Ge-II), the strength of each phase of germanium was analyzed with corresponding XRD peak widths. Besides the abnormal plastic behavior, unusual compressibilities from both phases at the mixture phase region are observed and the corresponding strain energy density is discussed.

In-situ high-pressure XRD measurements were carried out at 16BM-D station of the High-Pressure Collaborative Access Team (HPCAT), at the Advanced Photon Source, Argonne National Laboratory. The monochromatic x-ray beam at wavelength 0.4146 Å was focused to 12 μm (vertical) \times 7 μm (horizontal) in full width at half maximum (FWHM). A Mao-Bell type diamond anvil cell (DAC) with a pair of 300 μm culet sized diamond anvils was used to generate high pressure. The mixture of polycrystalline germanium fine grains and a small portion of gold powder were loaded into a 100- μm -diameter hole drilled in a stainless steel gasket, pre-indented to 40 μm thick. Gold powder was used as internal pressure standard. Each diffraction pattern was collected about 10 min after the pressure was adjusted and stabilized to ensure steady pressure during XRD measurements. The Raman spectrum measurements were conducted at a separate run using a He/Ne-mixed ion laser with a wavelength 633 nm. Ruby fluorescence shift was used to calibrate pressure. No pressure media were used in both experiments.

During compression, the structural phase transition of Ge-I to Ge-II started at 8.6 GPa and completed at 13.8 GPa, consistent with previous report under nonhydrostatic pressure.⁸ A typical XRD pattern and its Rietveld refinements of both Ge-I and Ge-II phases at 11.7 GPa were shown in Figure 1. We

^{a)}Authors to whom correspondence should be addressed. Electronic addresses: yangwg@hpstar.ac.cn and duanweihe@scu.edu.cn

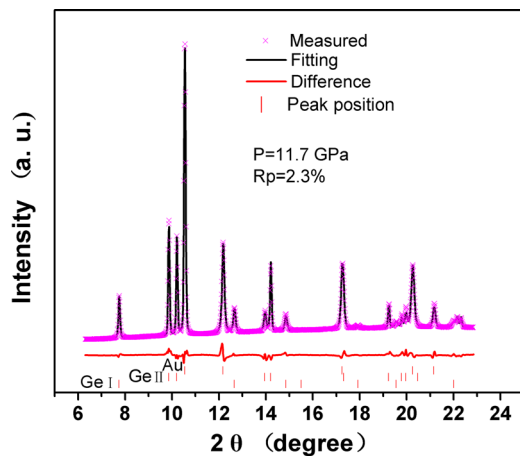


FIG. 1. A Rietvelt refinement of the powder x-ray diffraction pattern of Ge under 11.7 GPa. Both Ge-I and Ge-II phases are co-existed and fitted simultaneously.

name the pressure range 8.6 GPa to 13.8 GPa as the transition region. During decompression, the reversal transition was not observed down to 9.3 GPa.

Heterogeneous deviatoric strain at each grain of the powder sample, together with small grain size effect, give rise to diffraction peak broadening. In the case of angle dispersive X-ray diffraction, the following relation describes the grain size and strain dependence of diffraction line widths⁹

$$\text{FWHM}^2 \cos^2 \theta = \left(\frac{\lambda}{d} \right)^2 + \sigma^2 \sin^2 \theta, \quad (1)$$

where FWHM is the full-width at half-maximum of the diffraction profile on 2θ -scale. The symbols d , λ , and σ denote the grain size, X-ray wavelength, and deviatoric strain, respectively.

The deviatoric strains vs. pressure for Ge-I and Ge-II are plotted in Figure 2. Different from previous experimental observations or theoretical predictions, in which transformation induced either softening or hardening,^{1,6,10} the deviatoric strains of both Ge-I and Ge-II drop at the first half of

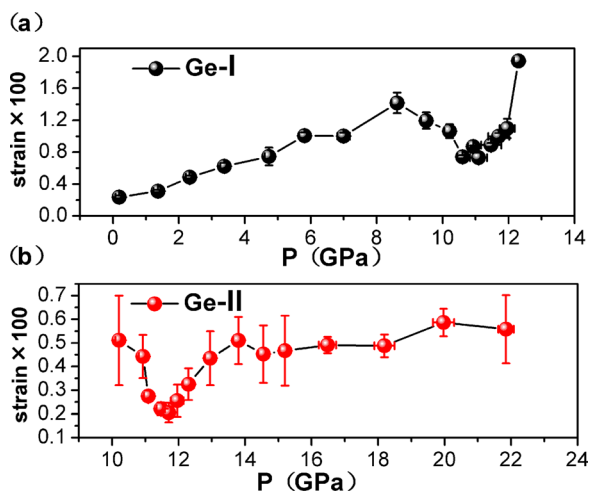


FIG. 2. Deviatoric strain of cubic diamond phase Ge-I (a) and β -tin phase Ge-II (b) versus pressure derived from Eq. (1).

the transformation region and then increase with pressure in the second half, which indicates a strain softening followed by a strain hardening. The deviatoric strain release of Ge-I could also be indicated by the Raman spectrum under pressure. Figure 3(a) shows the pressure evolution of FWHM of Raman peak, the decrease and increase of FWHM are in accordance with the soften and strengthen of Ge-I. Furthermore, the inflection points in FWHM of Raman peak versus pressure curve during phase transition is near 11 GPa, consisting with the XRD measurements.

Owing to the strong chemical bonding in it, germanium is a material easy to be softened after yield.⁷ The lattice misfit on the interface of Ge-I and Ge-II give rise to stress, and then, dislocations in the highly stressed zone near the interface can be annihilated,¹¹ resulting in the release of the strain in Ge-I and Ge-II simultaneously. In the perspective of energy, the strain energy resulted from the volume change accompanying transformation inhibits the phase transition by counteracting the chemical free energy driving force for growth. The plastic flow may relax this strain energy and enable growth to Ge-II grains.^{12,13} In addition, Ge-II grains started to nucleate near the grain boundaries and dislocation regions in the early stage of transition, where higher internal energy presents. This will consume some of the dislocations in Ge-I. In the latter stage, some nuclei of Ge-II particles will grow by minimizing the interfacial energy from the adjacent grains, which will create dislocations in Ge-II phase.¹⁴ These two factors may have influence on the strain evolution in the transition region considering the dislocation as the major source of deviatoric strain.¹⁵

As the volumetric change in phase transition of Ge-I to Ge-II is relatively large, it could be a proper model system for understanding how phase changes relate to deformation processes when olivine transforms to spinel, which is crucial to the transformational faulting model for deep-focus earthquakes.¹⁶ Deep-focus earthquakes occur at depths of 350–690 km in subducting lithosphere. The mechanism of them has been a puzzle since their discovery about 90 years ago.^{17,18} Based on the discovery and characterization of transformational faulting in several materials under nonhydrostatic stress, a model for

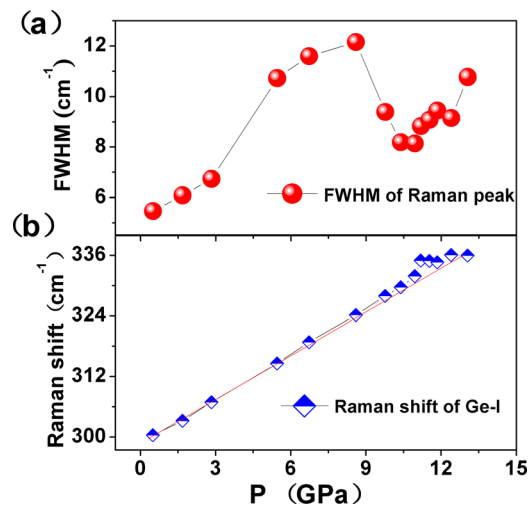


FIG. 3. Raman measurements of Ge-I during compression: FWHM of Raman peak (a) and Raman shift (b) versus pressure.

deep-focus earthquakes was proposed, in which the faults in deep-focus earthquakes are introduced by the olivine to spinel phase transition.¹⁹ However, the transformational faulting was observed in the quenched sample and it is not well understood how the faults formed and evolved under high pressure. Our *in situ* observations indicate that pressure induced phase transition can cause considerable reduction in the strength of each phase of material in the early stage of phase transition, and thereby promotes the formation and growth of fault. Additionally, in the second stage of phase transition the strength of each phase increases, which suggests the formation and growth of fault may be slowed down at this stage. Furthermore, if the strength of minerals in the subducting lithosphere follows the observation of germanium as demonstrated here (i.e., it reaches a minimum in the middle of transition and increases later) and the deep earthquake frequency is controlled by the strength of minerals, it could be speculated that earthquake frequency near the middle of transition zone is the highest while lower at the high pressure end of transition zone. This is indeed the situation of spatial distribution of deep earthquakes in transition zone.¹⁶

The lattice parameters of Ge-I and Ge-II phases versus pressure reveal anomalous patterns, as shown in Figure 4. During compression, the lattice parameters of Ge-I and Ge-II are distorted in the transition region. The lattice parameters a and c of Ge-II deviate to larger values from the normal compression curve. The lattice parameters of Ge-II are also anomalously larger than those observed during decompression at the same pressure range (Figs. 4(a) and 4(b)). There is no phase transition on Ge-II in this pressure range during decompression, which indicates a large hysteresis. Consequently, the a/c ratio of Ge-II in transition region shows significant deviation from that outside of the transition region (Fig. 4(c)). Meanwhile, the lattice parameter a of Ge-I in transition region deviated to lower value comparing with the low pressure trend (Fig. 4(d)). In other words, the lattices of Ge-II are stretched while the lattices of Ge-I is compressed in the transition region.

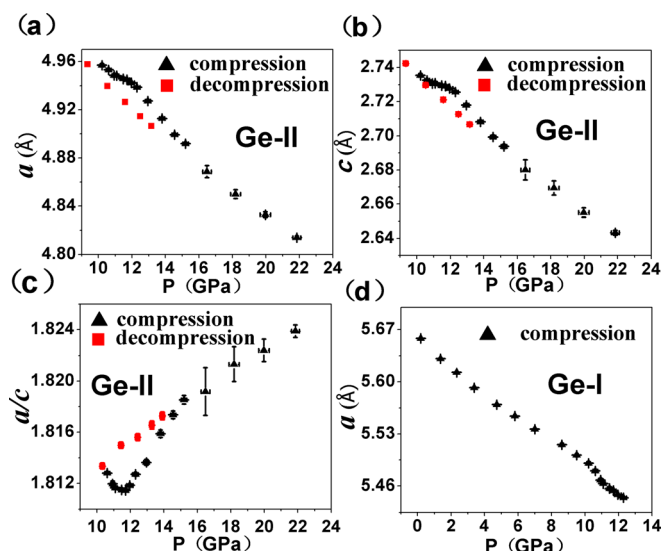


FIG. 4. The lattice parameters a (a), c (b), and a/c ratio (c) of the β -tin phase Ge-II and a (d) of cubic diamond phase Ge-I versus pressure.

The lattices distortions of Ge-I and Ge-II phases can be interpreted as a result of the volume misfit between the two coexisting phases. As the density of Ge-II is higher than Ge-I, the lattices of Ge-II are stretched to fit Ge-I, while the lattices of Ge-I are compressed. In the initial stage of transformation, the amount of Ge-II was small, the lattice parameter of Ge-I did not deviate significantly due to the relative small strained interface between Ge-I and Ge-II. Theoretical predictions point out that the nuclei always have an oblate shape which lowers the elastic energy at the beginning of phase transition.²⁰⁻²² For this reason, the misfit effect may be limited by the oblate shape of Ge-II and has little effect on the lattice parameters, resulting in the small deviation of lattice parameter of Ge-II at the beginning of phase transition. Near the end of transition, the amount of the Ge-II is dominant, the ratio of misfitted Ge-II to the unconstrained part decreases, hence, the lattice parameters of Ge-II calculated from powder XRD come back to normal compression condition.

The pressure-volume data for germanium are plotted in Figure 5. The data outside the phase transition region are fitted in terms of the third-order Birch-Murnaghan equation of state (EOS)²³

$$P = 1.5K \left[\left(\frac{V}{V_0} \right)^{-\frac{7}{3}} - \left(\frac{V}{V_0} \right)^{-\frac{5}{3}} \right] \times \left\{ 1 - 0.75(4 - K') \left[\left(\frac{V}{V_0} \right)^{\frac{2}{3}} - 1 \right] \right\}, \quad (2)$$

where $\frac{V}{V_0}$ is the ratio of unit cell volume at pressure P to that at ambient pressure. K is the bulk modulus at ambient condition and K' is its pressure derivative. The least-square fitting yields $K = 87.8$ (3.1) GPa and $K' = 5.9$ (1.2) for Ge-I, and $K = 95.8$ (12.3) GPa and $K' = 2.5$ (0.7) for Ge-II. As a nature result of the above-mentioned unusual lattice compression or stretching, the volumes of Ge-I and Ge-II in transition region are anomalously small or large, respectively.

We have also conducted *in-situ* high pressure Raman spectroscopy study to check the stretching mode of Ge-Ge bonding. During phase transition, the Raman peak of Ge-I

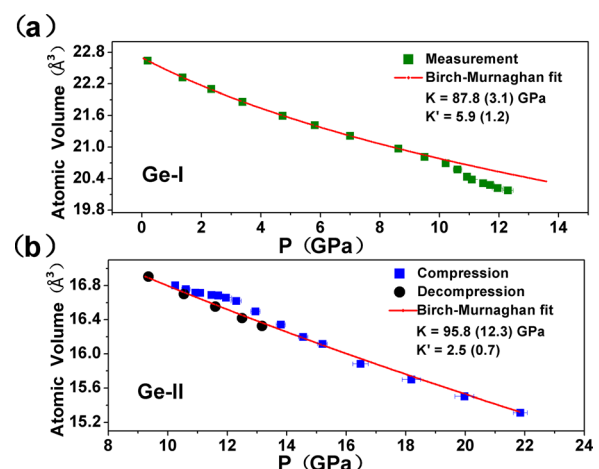


FIG. 5. Atomic volumes of cubic diamond phase Ge-I (a) and β -tin phase Ge-II (b) versus pressure.

shifts toward higher values comparing to the extension curve from the lower pressure shifts (Fig. 2(b)), indicating a shorter bonding distance, which is consistent with smaller unit cell volume observed by XRD.

A similar volume compressibility behavior was reported in the pressure-induced bcc-hcp phase transition of iron, where a lower effective pressure on the high pressure hcp nuclei was considered comparing with the pressure outside the sample.²⁴ Right after this, the hcp phase of iron was reported to be apparently distorted as a result of the lattice misfit during phase transition.²⁵ Combining these experimental observations and the current results, it could be speculated that, in an inclusion-host system during phase transition, the effective pressure on inclusion and host differs from that outside the sample due to the volume misfit. Thereby, the relative volume changes of them would be anomalous under pressure.

In the transition region, it should be addressed that both of the departures of the deviatoric strain and a/c ratio of Ge-II are relatively small at the beginning and end of transition comparing to the middle stage. Furthermore, the inflection point in deviatoric strain versus pressure curve of Ge-II is at 11.7 GPa, and similarly, the inflection point in lattice parameters versus pressure curves of Ge-II are at 11.7 GPa too. These consistencies also indicate that both of the strength and compressibility of Ge is controlled by the volume misfit during phase transition.

Following Eshelby,²⁶ the elastic strain energy induced by the volumetric strain can be expressed as

$$E = -\frac{1}{2}V\sigma\varepsilon, \quad (3)$$

where V is the volume of Ge-II, σ is the stress caused by volume misfit of the mixed phases which corresponds to the difference between the load pressure (P) and the pressure calculated from the equation of state of Ge-II (P_{II}) using the measured atomic volume, and ε is the strain when Ge-I transformed to Ge-II. The simplification here is that P and ε are uniform in Ge-II. If the shape of Ge-II nuclei keeps to be similar with that before transformation, then $\varepsilon = 1 - (V_{II}/V_I)^{1/3}$ (V_I and V_{II} are the atomic volume of Ge-I and Ge-II, respectively). The strain energy density of germanium during phase transition is obtained

$$E_v = \frac{E}{V} = \frac{1}{2}\alpha(P - P_{II}) \left[1 - \left(\frac{V_{II}}{V_I} \right)^{\frac{1}{3}} \right], \quad (4)$$

in which V is the total volume of sample, $\alpha = V_{II}/V$ and is the volume fraction of Ge-II (inset of Figure 6). Figure 6 shows the pressure dependence of strain energy density in the mixed phase system during transformation. The strain energy density is relative small at the beginning of transformation and increases with the progress of phase transition until reaches to the highest value about $3 \times 7^{10} \text{ J/m}^3$, after this it decreases with the progress of phase transition to nearly zero, in agreement with compression behaviors described above.

The *in-situ* high pressure XRD and Raman spectroscopy observation of germanium at transition region show that the

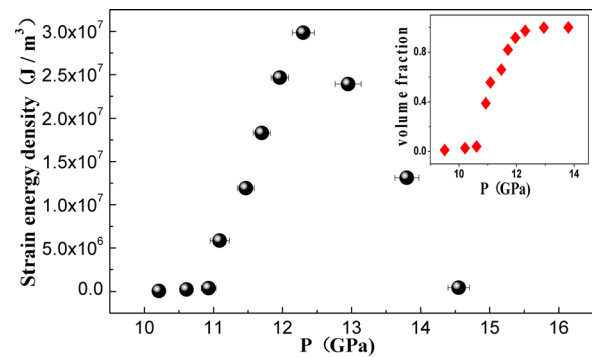


FIG. 6. Strain energy density of germanium versus pressure during phase transition, the inset shows the volume fraction of β -tin phase Ge versus pressure.

plasticity and compressibility of the mixed cubic-diamond and β -tin phases behave unusually. Each phase of germanium experiences strain softening at the beginning of transition and strain hardening latter. Furthermore, the volume of the low density phase (Ge-I) shrinks, while the high density phase (Ge-II) is inflated during phase transformation. These findings are essential for understanding the fundamental mechanisms of solid state phase transformation. Moreover, they may have implications for the transformation plasticity in materials and contribute to the understanding the seismicity of the transition zone in Earth.

This work was supported by the China 973 Program (Grant No. 2011CB808200) and National Natural Science Foundation of China (Grant No. 11027405). W.Y. and H.-K.M. acknowledge the financial support from DOE-BES X-ray Scattering Core Program under Grant No. DE-FG02-99ER45775. HPCAT operations are supported by DOE-NNSA under Award Nos. DE-NA0001974 and DOE-BES under Award No. DE-FG02-99ER45775, with partial instrumentation funding by NSF. APS is supported by DOE-BES, under Contract No. DE-AC02-06CH11357.

¹G. W. Greenwood and R. H. Johnson, *Proc. R. Soc. London, Ser. A* **283**, 403 (1965).

²P. Fratzi, O. Penrose, and J. L. Lebowitz, *J. Stat. Phys.* **95**, 1429 (1999).

³S. J. Song, F. Liu, and Z. H. Zhang, *Acta Mater.* **64**, 266 (2014).

⁴S. R. Meka, K. S. Jung, E. Bischoff, and E. J. Mittemeijer, *Philos. Mag. Lett.* **92**, 1435 (2012).

⁵S. R. Meka, E. Bischoff, B. Rheingans, and E. J. Mittemeijer, *Philos. Mag. Lett.* **93**, 238 (2013).

⁶D. C. Dunand and C. M. Bedell, *Acta Mater.* **44**, 1063 (1996).

⁷S. Karato, *Deformation of Earth Materials: An Introduction to The Rheology of Solid Earth* (Cambridge University Press, New York, 2008), p. 280.

⁸C. S. Menoni, J. Z. Hu, and I. L. Spain, *Phys. Rev. B* **34**, 362 (1986).

⁹A. K. Singh, A. Jain, H. P. Liermann, and S. K. Saxena, *J. Phys. Chem. Solids* **67**, 2197 (2006).

¹⁰S. V. Panasyuk and B. H. Hager, *Geophys. J. Int.* **133**, 741 (1998).

¹¹Y. Y. Earmme, W. C. Johnson, and J. K. Lee, *Metall. Trans. A* **12**, 1521 (1981).

¹²J. L. Mosenfelder, J. A. Connolly, D. C. Rubie, and M. Liu, *Phys. Earth Planet. Inter.* **120**, 63 (2000).

¹³T. Kubo, E. Ohtani, T. Kato, T. Shinmei, and K. Fujino, *Science* **281**, 85 (1998).

¹⁴R. L. Penn and J. F. Banfield, *Science* **281**, 969 (1998).

¹⁵T. Ungár and G. Tichy, *Phys. Status Solidi A* **171**, 425 (1999).

¹⁶S. H. Kirby, W. B. Durham, and L. A. Stern, *Science* **252**, 216 (1991).

¹⁷H. H. Turner, *Geophys. J. Int.* **1**(s1), 1 (1922).

¹⁸K. Wadati, *Geophys. Mag.* **1**, 162 (1928).

- ¹⁹H. W. Green and H. Houston, *Annu. Rev. Earth Planet. Sci.* **23**, 169 (1995).
- ²⁰E. A. Brener, S. V. Iordanskii, and V. I. Marchenko, *Phys. Rev. Lett.* **82**, 1506 (1999).
- ²¹L. Zhang, L. Q. Chen, and Q. Du, *Phys. Rev. Lett.* **98**, 265703 (2007).
- ²²F. R. N. Nabarro, *Proc. R. Soc. London, Ser. A* **175**, 519 (1940).
- ²³F. Birch, *J. Geophys. Res.* **83**, 1257, doi:10.1029/JB083iB03p01257 (1978).
- ²⁴A. P. Jephcoat, H. K. Mao, and P. M. Bell, *J. Geophys. Res.* **91**, 4677, doi:10.1029/JB091iB05p04677 (1986).
- ²⁵W. A. Bassett and E. Huang, *Science* **238**, 780 (1987).
- ²⁶J. D. Eshelby, *Proc. R. Soc. London, Ser. A* **241**, 376 (1957).